EUROPHYSICS LETTERS 15 November 2004

Europhys. Lett., **68** (4), pp. 557–563 (2004)
DOI: 10.1209/epl/i2004-10240-4

Hard X-ray core-level photoemission of V_2O_3

N. Kamakura[1], M. Taguchi[1], A. Chainani[1], Y. Takata[1], K. Horiba[1], K. Yamamoto[1], K. Tamasaku[2], Y. Nishino[2], D. Miwa[2], E. Ikenaga[3], M. Awaji[3], A. Takeuchi[3], H. Ohashi[3], Y. Senba[3], H. Namatame[4], M. Taniguchi[4], T. Ishikawa[2], K. Kobayashi[3] and S. Shin[1,5]

[1] *Soft X-ray Spectroscopy Laboratory, RIKEN/SPring-8 Mikazuki-cho, Sayo-gun, Hyogo 679-5148, Japan*
[2] *Coherent X-ray Optics Laboratory, RIKEN/SPring-8 Mikazuki-cho, Sayo-gun, Hyogo 679-5148, Japan*
[3] *JASRI/SPring-8 - Mikazuki-cho, Sayo-gun, Hyogo 679-5198, Japan*
[4] *HiSOR, Hiroshima University - Higashi-Hiroshima, Hiroshima 739-8526, Japan*
[5] *Institute for Solid State Physics, University of Tokyo Kashiwa, Chiba 277-8581, Japan*

received 10 August 2004; accepted in final form 24 September 2004
published online 27 October 2004

PACS. 71.30.+h – Metal-insulator transitions and other electronic transitions.
PACS. 79.60.-i – Photoemission and photoelectron spectra.

Abstract. – We study the Mott-Hubbard metal-insulator transition in single-crystal V_2O_3 using hard X-ray (HX : $h\nu = 5940\,\mathrm{eV}$) core-level photoemission spectroscopy (PES). HX-PES enables a bulk probe of the electronic structure in the paramagnetic metallic and antiferromagnetic insulating phases. Metallic V_2O_3 shows additional features at low binding energy to the main peak of V $1s$, $2p$, and $3s$ core levels, which vanish in the insulating phase. The low-binding-energy features in the metallic phase are also observed using soft X-rays (SX : $h\nu = 1450\,\mathrm{eV}$), but with a reduced relative intensity compared to the HX-PES spectrum. A model cluster calculation including core hole screening by coherent states at the Fermi level, reproduces the low-binding-energy features in the metallic phase. The O $1s$ core level also shows spectral changes: the asymmetric line shape in the metallic phase transforms to a symmetric line shape in the insulating phase, consistent with the metal-insulator transition. The results indicate screening by coherent states is more effective in the bulk compared to the surface. HX-PES is, thus, a reliable probe of the electronic-structure changes across the metal-insulator transition in strongly correlated electron systems.

Introduction. – V_2O_3 represents a typical Mott-Hubbard system and has been extensively studied over the past several decades [1]. The metal-insulator transition (MIT), which occurs at $T_{\mathrm{MI}} = 160\,\mathrm{K}$, transforms V_2O_3 from an antiferromagnetic insulator (AFI) to a paramagnetic metal (PM). It is associated with a structural transformation from the trigonal (corundum) symmetry of the PM phase to a monoclinic structure at low temperature [2–6]. The formal oxidation state of V ions is V^{3+} with $3d^2$ configuration, where the two electrons occupy the t_{2g} orbitals. Due to a trigonal distortion of the V_2O_3 lattice, the t_{2g} orbital splits into

nondegenerate a_{1g} and doubly degenerate e_g^π orbitals. While an early work had pictured a ($S = 1/2$) singlet formation with $\{e_g^\pi, a_{1g}\}$ configuration due to pairing of two adjacent V ions $\{V_1, V_2\}$ along the c-axis [7], recent work indicates that the orbital configuration is better written as an admixture of $\{e_g^\pi, e_g^\pi\}$ and $\{e_g^\pi, a_{1g}\}$ configurations and the two electrons in a V^{3+} ion form a high-spin ($S = 1$) state [8–11].

Several PES experiments have been done to study the electronic structure of V_2O_3 [12–21]. Valence band studies using ultraviolet photoemission spectroscopy (UPS) have shown that the O $2p$ band is located between ~ 4 and ~ 10 eV binding energies and the V $3d$ states lie within ~ 3 eV from the Fermi level (E_F) [12,13]. The V $3d$ states show significant changes across the MIT with the formation of a gap in the AFI phase [12,13]. However, only recent valence band experiments using soft X-rays showed a prominent E_F peak, the so-called coherent peak in the PM phase of V_2O_3 [14]. The coherent peak appears across the insulator-to-metal transition with a rearrangement of spectral weight from the lower and upper Mott-Hubbard bands as a function of U/W (U: on-site Coulomb correlation energy; W: effective bandwidth), as is well described by a dynamical mean-field theory of V_2O_3 [11]. Core-level PES is also a powerful tool to study electronic states of transition metal oxides. Early studies of the V $2p$ and $2s$ PES showed [15–18] that the spectra can be well reproduced by cluster calculations indicating strong hybridization between O $2p$ and V $3d$ states. This hybridization leads to considerable weight for the charge transfer configurations $d^3\underline{L}, d^4\underline{L}^2, \ldots$ with a net d-electron number $n_d \sim 2.6$ in the ground state and explains the observed charge transfer satellites in the core-level PES spectra [15–18]. Temperature-dependent V $2p$ core-level studies using SX-PES showed a weak low-binding-energy feature to the main peak [19, 20]. Since the low-binding-energy feature was observed only in the metallic phase, it was attributed to metallic screening. Recently, HX-PES has been developed as a genuine probe of the bulk (50–100 Å) electronic structure [22–27]. The role of surface *vs.* bulk electronic structure in three-dimensional correlated electron systems has attracted significant interest recently [28–31].

Here, we have applied HX-PES ($h\nu = 5940$ eV) to study the V $1s$, $2p$, and $3s$ core-levels of the PM and AFI phases of pure V_2O_3. For V $2p$ core levels, we make a comparison of the HX-PES ($h\nu = 5940$ eV) spectrum with the SX-PES ($h\nu = 1450$ eV) spectrum in order to elucidate the differences due to the probing depth. The electron mean free path (MFP) of photoelectrons with 5425 eV kinetic energy, which corresponds to the kinetic energy of photoelectrons from V $2p$ core levels when excited with a photon energy of 5940 eV, is estimated to be about ~ 80 Å. This is about 4 times larger than the MFP (~ 20 Å) of photoelectrons obtained using AlK_α photons ($h\nu = 1486.6$ eV) [32], the photon energy used in early SX-PES studies. Another important advantage of HX-PES is that a deep core level can be studied, which is not possible with a conventional PES experiment using AlK_α photons. For example, the V $1s$ core level is located at about 5465 eV binding energy, and can be probed only using hard X-rays. Furthermore, the $1s$ state is expected to possess a simpler shape, since the exchange splitting is expected to be negligible in V $1s$ spectra due to the much smaller overlap between $1s$ and $3d$ orbitals, as compared to the usually observed exchange splitting in $3s$ spectra of $3d$ transition metal compounds using SX-PES [33–36]. The present study of V $1s$, $2p$, and $3s$ core levels as a function of temperature provides clear evidence for the metal-insulator transition, with the observation of low-binding-energy well-screened features in the PM phase which are absent in the AFI phase. A model cluster calculation including a screening channel due to coherent states at E_F reproduces the low-binding-energy features well. The O $1s$ core level also shows a line shape consistent with the MIT.

Experiment. – HX-PES experiments were performed at an undulator beamline, BL47XU, of SPring-8. The experimental details are described in refs. [22, 23]. Since the electron emis-

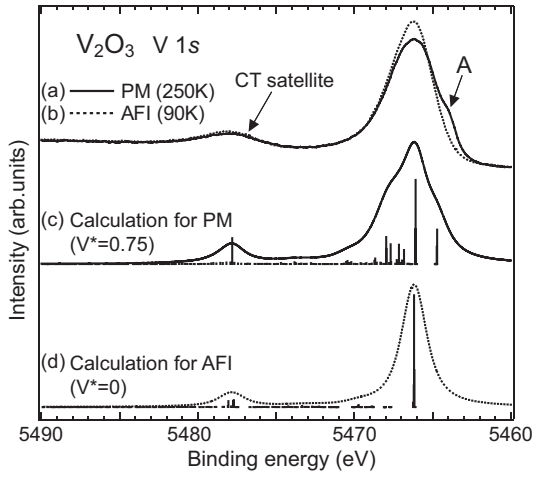

Fig. 1 – V 1*s* PES spectra of the (a) PM (250 K) and (b) AFI (90 K) phases measured with $h\nu =$ 5940 eV, where the intensities are normalized by the area under the curves. The calculations including the screening from coherent states are also included in (c) and (d) for the PM ($V^* = 0.75$) and AFI ($V^* = 0$) phases.

sion angle was set to 70° relative to the sample surface, the probing depth is estimated to be 70 Å [32]. SX-PES experiments were performed at an undulator beamline, BL17SU of SPring-8, using a photon energy of 1450 eV obtained by a grating monochromator. The total energy resolution was set to about 400 meV for both, the HX and SX-PES measurements. The V_2O_3 single-crystal sample was fractured in a vacuum of better than 2×10^{-7} Pa for HX-PES and 2×10^{-8} Pa for SX-PES experiments.

Results and discussion. – Figure 1 shows the V 1*s* PES spectra of V_2O_3 in (a) the PM (250 K) and (b) the AFI (90 K) phases measured with $h\nu = 5940$ eV. The spectra are normalized for the area under the curve over the measured energy range. The observed V 1*s* spectrum shows a clear temperature dependence across the MIT. At a lower binding energy to the main peak in the PM phase, a shoulder structure is observed, which is labelled A. The feature A disappears in the AFI phase. This temperature dependence across the MIT in V_2O_3 indicates that the feature A is strongly related to the conductivity of V_2O_3, *i.e.*, the density of states at E_F. Since the valence band PES spectrum of V_2O_3 has shown a prominent coherent peak at E_F [14], which collapses in the AFI phase [11], it is important to consider an additional screening channel from the coherent V 3*d* states at E_F to explain the observed behaviour.

In order to understand the origin of the feature A in the PM phase, we have carried out a cluster model calculation as is usually done for core-level spectra of transition metal compounds, and including an additional screening channel for charge transfer from coherent states at E_F. The calculation is described in detail elsewhere [26]. The present calculation employs a VO_6 cluster in the C_{3v} local symmetry with full multiplet structure. The charge transfer energy from coherent states to the upper Hubbard (UH) band Δ^*, approximated as levels, is defined as the energy difference between the configuration averaged energies $E(3d^3\underline{C}) - E(3d^2)$. The usual charge transfer energy Δ is the energy difference between the ligand states and the UH band. The ground state is described by a linear combination of the following configurations: $3d^2$, $3d^3\underline{L}$, $3d^4\underline{L}^2$, $3d^1C$, $3d^3\underline{C}$, $3d^4\underline{LC}$, and $3d^4\underline{C}^2$, where C, $\underline{C}$ and $\underline{L}$ represent the electron in the coherent states just above E_F, the hole in the coherent states just below E_F

and the hole in O $2p$ ligand band, respectively. The final states are described by a linear combination of $1s^1 3d^2$, $1s^1 3d^3\underline{L}$, $1s^1 3d^4\underline{L}^2$, $1s^1 3d^1 C$, $1s^1 3d^3\underline{C}$, $1s^1 3d^4\underline{LC}$, and $1s^1 3d^4\underline{C}^2$. An effective coupling parameter $V^*(e_g)$, for describing the interaction strength between the V $3d$ orbitals and coherent states is introduced, analogous to the hybridization $V(e_g)$ between the V $3d$ orbitals and ligand states. Figure 1(c) shows the calculated result for the PM phase. In the calculation, the following parameters are used: $U = 4.5$, $\Delta = 6.0$, $U_{dc} = 6.5$, $10Dq = 1.2$, $\Delta_{trg} = -0.05$, $V(e_g) = 2.9$, $\Delta^* = 0.9$, $V^*(e_g) = 0.75$, in units of eV, where the definition of these parameters are described in ref. [26]. The overall spectral features of V $1s$ across the MIT are well reproduced in the calculation. An analysis of the final states shows that $1s^1 3d^2$ states form the main peak. The $1s^1 3d^3\underline{C}$ state lies below these states, because Δ^* is much smaller than Δ, and constitutes the feature A. Therefore, the feature A originates from screening by the coherent states at E_{F}. This, in turn, should mean that the absence of the feature A in the AFI phase indicates the collapse of the coherent states, as is also theoretically predicted [11]. This is actually confirmed by the calculation with $V^* = 0$, which suppresses the screening from coherent states, keeping all other parameter values to be the same. The calculation reproduces the observed symmetric V $1s$ spectrum in the AFI phase including the disappearance of the feature A (fig. 1(d)), but for the width of the main peak obtained in the experiment.

Another interesting observation in the V $1s$ spectra of figs. 1(a) and (b), is the existence of a satellite structure at 5478 eV binding energy, which does not show temperature dependence, in contrast to the clear temperature dependence of the feature A. The calculation also reproduces the satellite structure as a charge transfer (CT) satellite formed by the $1s^1 3d^3\underline{L}$ state, and which does not depend on the coupling V^* with the coherent states. The unchanged CT

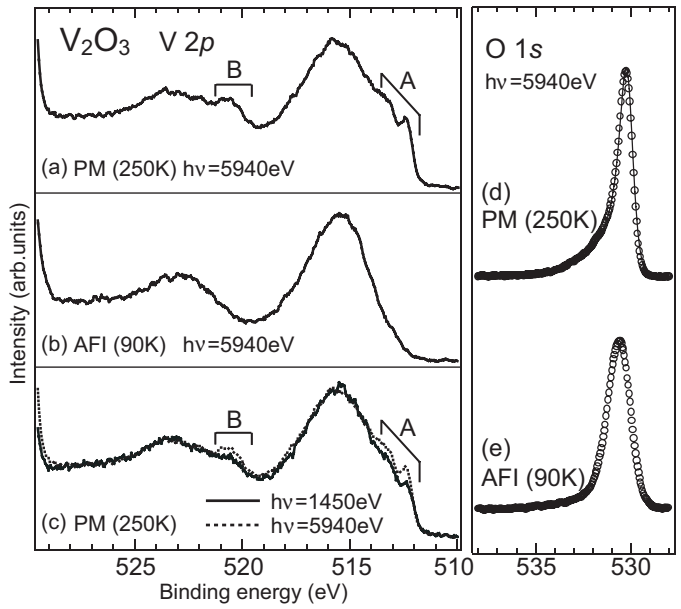

Fig. 2 – V $2p$ PES spectra of V_2O_3 in the (a) PM (250 K) and (b) AFI (90 K) phases measured with $h\nu = 5940$ eV. (c) V $2p$ PES spectra of V_2O_3 in the PM (250 K) with $h\nu = 1450$ and 5940 eV are shown by solid and broken curves, respectively. O $1s$ PES spectra of V_2O_3 in the (d) PM (250 K) and (e) AFI (90 K) phases with $h\nu = 5940$ eV are also shown by empty circles. For the PM phase (d), the thin solid line shows the Doniach-Šunjić curve fit result.

satellite as a function of temperature (figs. 1(a) and (b)) indicates that the O $2p$ and UH bands energy separation does not change across the metal-insulator transition.

Figures 2(a) and (b) show the V $2p$ PES spectra of V_2O_3 in the PM phase (250 K) and AFI phase (90 K) measured with $h\nu = 5940$ eV, respectively. The V $2p$ spectrum of the PM phase (fig. 2(a)) shows a markedly different spectral shape from the one reported using AlK_α photons [15–18]. At lower binding energy of the V $2p_{3/2}$ main peak, there is a shoulder and a very sharp peak, which are again labelled as A. V $2p_{1/2}$ also shows the structure at low binding energy (labelled B). In the AFI phase, the features A and B completely vanish like the feature A in V $1s$ spectra. The features A and B also originate from the screening by coherent states ($1s^1 3d^3 \underline{C}$) as has been recently shown for $V_{1.98}Cr_{0.02}O_3$ [26]. The observed low-binding-energy features, especially the feature A in the $2p_{3/2}$ region are much sharper than the low-binding-energy feature in V $1s$. This is suggested to be due to the larger lifetime broadening in V $1s$. The V $2p$ spectrum of the PM phase (250 K) with $h\nu = 1450$ eV also shows the low-binding-energy features A and B, which are observed at same energy position as in the HX-PES spectrum (fig. 2(c)). The previous V $2p$ PES studies using soft X-rays for V_2O_3 cleaved in ultrahigh vacuum or for thin films have reported a broad weak structure at low binding energies to the main peak, but the sharp feature in A has not been observed [19–21]. The present HX-PES and SX-PES comparison on the same single crystals indicates that the intensities of the features A and B are larger in the HX-PES spectrum. The intensity reduction on decreasing the photon energy from 5940 eV to 1450 eV is related to the probing depth decreasing from ~ 70 Å to ~ 20 Å. The clear observation of sharp features in the HX-PES spectrum is thus attributed to the larger probing depth as well as to better resolution compared to the earlier study. The present study indicates that screening by coherent states at E_F is more effective in the bulk-sensitive measurement. It has been shown that nonlocal or nonconventional screening effects are modified at the surface compared to the bulk [37], consistently with the present results. The probing depth of the V $2p$ spectrum with $h\nu = 1450$ eV is rather near that of the V $1s$ spectrum in fig. 1. The appearance of the sharp low-binding-energy feature in the V $2p$ spectrum even with $h\nu = 1450$ eV excludes the possibility of the surface contribution for the broad feature of A in the V $1s$ spectrum.

The O $1s$ core level with $h\nu = 5940$ eV shows an asymmetric shape in the PM phase (fig. 2(d)) which becomes symmetric in the AFI phase (fig. 2(e)). An asymmetric line shape is known to result from continuous excitations at E_F, which is described as the Doniach and Šunjić line shape [38]. A curve fit was made to estimate the singularity index (α) of the Doniach and Šunjić line shape [38], shown in fig. 2(d) as a thin solid line. The curve fit matches well

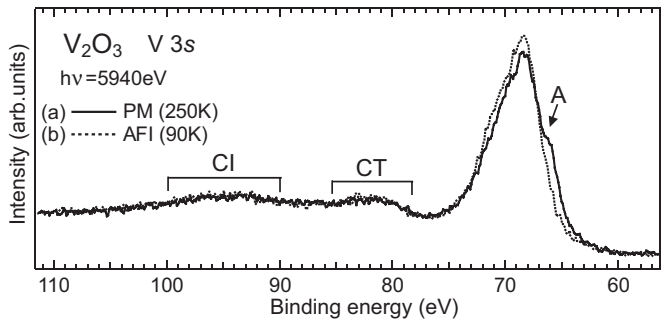

Fig. 3 – V $3s$ PES spectra of the (a) PM (250 K) (solid curve) and (b) AFI (90 K) (broken curve) phases with $h\nu = 5940$ eV.

with the experimental spectrum, from which we have obtained the value of α to be 0.248 in the PM phase. The observed change in the line shape from an asymmetric to symmetric behaviour in the PM and AFI phases, respectively, is consistent with the temperature-dependent metal-insulator transition. The O 1s spectra do not show a low-binding-energy feature as in the V 1s and 2p states, suggesting that the additional screening channel at $E_{\rm F}$, forming the low-binding-energy feature, is operative only in the V derived states.

Finally, we discuss the V 3s core-level PES spectra of the AFI and PM phases with $h\nu = 5940\,\text{eV}$ as shown in figs. 3(a) and (b). The data are normalized for the area under the curve. The observed V 3s spectra show temperature-dependent changes related to the feature A at low binding energy to the main peak, as seen in fig. 3. The feature A was not observed in V 3s core levels using AlK_α [16]. The peak A vanishes in the AFI phase (fig. 3(b)), as in the V 1s and 2p spectra. The V 3s spectra show two broad satellite structures at $\sim 81\,\text{eV}$ and $\sim 94\,\text{eV}$, which are centred at 13 eV and 26 eV from the main peak. The V 3s spectrum using AlK_α also showed the 81.4 eV binding energy peak at the same energy position and concluded it to be a CT satellite [16]. The satellite at $\sim$ 94 eV is assigned to configuration interaction (CI) between $3s^1 3p^6 3d^n$ and $3s^2 3p^4 3d^{n+1}$ final states, as predicted by cluster calculations [17]. Both, the CT and CI satellites, do not show temperature dependence. This behaviour is consistent with the fact that the CI satellite has an atomic origin [39, 40], while the CT satellite position is a measure of the separation between the O 2p states and the UH band which does not change across the MIT transition.

Conclusion. – In conclusion, we have performed a HX-PES study of the Mott-Hubbard transition as manifested in the V 1s, 2p, and 3s core levels of V_2O_3. The observed core-level spectra show well-screened features at low binding energy to the main peak in the PM phase. The low-binding-energy features vanish in the AFI phase. A model cluster calculation confirms that the low-binding-energy feature originates from screening by the coherent states at $E_{\rm F}$. The absence of the low-binding-energy feature in the AFI phase indicates the additional screening channel in the PM phase and a collapse of the coherent states at $E_{\rm F}$ in the AFI phase of V_2O_3. The low-binding-energy feature is also observed in the V 2p spectrum of the PM phase of V_2O_3 using $h\nu = 1450\,\text{eV}$ photons, but with reduced intensity. The O 1s core level also shows changes of the spectral shape from an asymmetric line shape in the PM phase to a symmetric feature in the AFI phase, confirming the MIT. The CT and CI satellites observed in the V 1s and 3s core levels do not show temperature dependence, in contrast to the low-binding-energy well-screened feature. The results show that hard X-ray core-level PES is an important and reliable tool to study the MIT in correlated electron systems.

* * *

We thank Drs. T. Takeuchi, M. Arita and J. J. Kim for help with experiments and Profs. K. Katsumata, S. W. Lovesey and T. Yokoya for valuable discussions.

REFERENCES

[1] Mott N. F., *Metal-Insulator Transitions* (Taylor & Francis, London) 1990; Cox P. A., *Transition Metal Oxides: An Introduction to their Electronic Structure and Properties* (Clarendon Press, Oxford) 1992; Imada M., Fujimori A. and Tokura Y., *Rev. Mod. Phys.*, **70** (1998) 1039.
[2] McWhan D. B. *et al.*, *Phys. Rev. Lett.*, **27** (1971) 941.
[3] Kuwamoto H. *et al.*, *Phys. Rev. B*, **22** (1980) 2626.

[4] Warekois E. P., *J. Appl. Phys.*, **31** (1960) 346S.
[5] Dernier P. D. and Marezio M., *Phys. Rev. B*, **2** (1970) 3771.
[6] Robinson W. R., *Acta Crystallogr., Sect. B*, **31** (1970) 1153.
[7] Castellani C., Natoli C. R. and Ranninger J., *Phys. Rev. B*, **18** (1978) 4945.
[8] Park J.-H. *et al.*, *Phys. Rev. B*, **61** (2000) 11506.
[9] Paolasini L. *et al.*, *Phys. Rev. Lett.*, **82** (1999) 4719.
[10] Moon R. M., *Phys. Rev. Lett.*, **25** (1970) 527.
[11] Georges A. and Krauth W., *Phys. Rev. B*, **48** (1993) 7167; Ezhov S. Yu., Anisimov V. I., Khomskii D. I. and Sawatzky G. A., *Phys. Rev. Lett.*, **83** (1999) 4136; Mila F. *et al.*, *Phys. Rev. Lett.*, **85** (2000) 1714; Held K., Keller G., Eyert V., Vollhardt D. and Anisimov V. I., *Phys. Rev. Lett.*, **86** (2001) 5345; Di Matteo S., Perkins N. B. and Natoli C. R., *Phys. Rev. B*, **65** (2002) 054413.
[12] Shin S. *et al.*, *J. Phys. Soc. Jpn.*, **64** (1995) 1230.
[13] Shin S. *et al.*, *Phys. Rev. B*, **41** (1990) 4993.
[14] Mo S.-K. *et al.*, *Phys. Rev. Lett.*, **90** (2003) 186403.
[15] Bocquet A. E. *et al.*, *Phys. Rev. B*, **53** (1996) 1161.
[16] Zimmermann R., Claessen R., Reinert F., Steiner P. and Hüfner S., *J. Phys. Condens. Matter*, **10** (1998) 5697.
[17] Uozumi T., Okada K. and Kotani A., *J. Phys. Soc. Jpn.*, **62** (1993) 2595.
[18] Sawatzky G. A. and Post D., *Phys. Rev. B*, **20** (1979) 1546.
[19] Henrich V. E. and Cox P. A., *The Surface Science of Metal Oxides* (Cambridge University Press, Cambridge) 1994; Kurtz R. L. and Henrich V. E., *Phys. Rev. B*, **28** (1983) 6699; Smith K. E. and Henrich V. E., *Phys. Rev. B*, **50** (1994) 1382.
[20] Toledano D. S., Metcalf P. and Henrich V. E., *Surf. Sci.*, **449** (2000) 19.
[21] Rata A. D. *et al.*, *Phys. Rev. B*, **69** (2004) 075404.
[22] Kobayashi K. *et al.*, *Appl. Phys. Lett.*, **83** (2003) 1005.
[23] Takata Y. *et al.*, *Appl. Phys. Lett.*, **84** (2004) 4310.
[24] Chainani A. *et al.*, *Phys. Rev. B*, **69** (2004) 180508(R).
[25] Kobayashi K. *et al.*, *Jpn. J. Appl. Phys.*, **43** (2004) L1029.
[26] Taguchi M. *et al.*, Preprint cond-mat/0404200.
[27] Horiba K. *et al.*, Preprint cond-mat/0405442.
[28] Braicovich L. *et al.*, *Phys. Rev. B*, **56** (1997) 15047.
[29] Liebsch A. *et al.*, *Phys. Rev. Lett.*, **90** (2003) 096401.
[30] Sekiyama A. *et al.*, *Nature*, **403** (2000) 396.
[31] Kamakura N. *et al.*, *Europhys. Lett.*, **67** (2004) 240.
[32] NIST Electron Inelastic-Mean-Free-Path Database:Ver. 1.1 (2000).
[33] van Vleck J. H., *Phys. Rev.*, **45** (1934) 405.
[34] van Acker J. F. *et al.*, *Phys. Rev. B*, **37** (1988) 6827.
[35] Shin S. *et al.*, *Phys. Rev. B*, **46** (1992) 9224.
[36] Park K.-H. *et al.*, *Phys. Rev. B*, **53** (1996) 5633.
[37] van Veenendaal M. A. and Sawatzky G. A., *Phys. Rev. Lett.*, **70** (1993) 2459; van den Brink J. and Sawatzky G. A., *Europhys. Lett.*, **50** (2000) 447; Hesper R., Tjeng L. H. and Sawatzky G. A., *Europhys. Lett.*, **40** (1997) 177.
[38] Doniach S. and Šunjić M., *J. Phys. C*, **3** (1970) 285.
[39] Bagus P. S., Freeman A. J. and Sasaki F., *Phys. Rev. Lett.*, **30** (1973) 850.
[40] Okada K. and Kotani A., *J. Phys. Soc. Jpn.*, **61** (1992) 4619.